The effect of the front-to-rear wheel torque distribution on vehicle handling: an experimental assessment

F. Bucchi
Dipartimento di Ingegneria Civile e Industriale, Università di Pisa, Pisa, Italy

B. Lenzo
Department of Engineering and Mathematics, Sheffield Hallam University, Sheffield, UK

F. Frendo
Dipartimento di Ingegneria Civile e Industriale, Università di Pisa, Pisa, Italy

A. Sorniotti
Centre for Automotive Engineering, University of Surrey, Guildford, UK

ABSTRACT: The front-to-rear wheel torque distribution influences vehicle handling and, ultimately, it affects key factors such as vehicle safety and performance. At a glance, due to part of the available tire-road friction being used for traction at the driven axle, a Front-Wheel-Drive (FWD) vehicle would be expected to be more understeering than a Rear-Wheel-Drive (RWD) vehicle. However, such effect may be counterbalanced, or even reversed, mainly due to the yaw moment caused by the lateral contribution of the traction forces at the front wheels. This paper proposes an experimental assessment, carried out on a fully electric vehicle with multiple motors, allowing different front-to-rear wheel torque distributions. The results confirm that the yaw moment effect discussed is considerable, especially at low vehicle speeds and high steering angles. In particular, the RWD vehicle resulted more understeering than the FWD one at 30 km/h.

1 INTRODUCTION

The handling of a vehicle is a key factor for both safety and performance. Since the 1970s the turning response has been studied, firstly through linearized single-track models for steady-state conditions under the hypotheses of small slip and steering angles, introducing the handling diagram and the understeer coefficient (Pacejka 1973). Later on, several analyses were proposed on Direct Yaw moment Control (DYC) (Shibahata 1993, van Zanten 2000), i.e a technique aimed at enhancing the vehicle handling by controlling the brake or drive torques at each wheel. In first instance DYC was not related to the handling diagram approach, as it was applied in non-steady state conditions (e.g. as Electronic Stability Control, ESC). Recently (De Novellis et al. 2014, De Novellis et al. 2015, Lenzo et al. 2016, Lenzo et al, in press) proposed direct yaw moment control algorithms which are active continuously, and not only in emergency conditions, with the specific purpose of designing the handling characteristic of the vehicle. Although such analyses were performed with electric vehicles with independent motors and no differential, it is important to consider that longitudinal forces affect the vehicle turning dynamics also in conventional vehicles depending on the differential type or working condition (Frendo et al. 2006, Frendo et al. 2007).

More recently, (Bucchi & Frendo 2016) proposed a method to relate the steady-state vehicle behavior, described by the handling diagram, to the whole yaw moment resulting from tire actions, in quasi-steady state maneuvers that can be easily performed by real vehicles, not necessarily equipped with a DYC feature. The paper proposed a detailed yaw moment analysis, assessing the influence of the individual yaw moment contributions (e.g., related to lateral forces, longitudinal forces, etc.) on the vehicle handling and over/understeer, finding out remarkable differences among Front-, Rear- and All-Wheel-Drive architectures (FWD, RWD and AWD, respectively). In particular, with reference to a steering pad maneuver, the RWD equipped vehicle resulted more understeering than the FWD and AWD ones, that is contrary to the common belief (Osborn & Shim 2006). These findings were only supported by multibody simulations, whilst an experimental proof appears to be missing in the literature.

The main contribution of this paper is the experimental validation of the analysis proposed in (Bucchi & Frendo 2016). Several ramp steer maneuvers were performed with a fully electric vehicle with multiple motors, i.e. with a torque vectoring feature allowing the selection of any front-to-rear wheel torque distribution. The effect of FWD, RWD and AWD layouts on the handling diagram is presented and discussed.

2 TEST EQUIPMENT AND PROCEDURE

This experimental study was conducted on the fully electric Range Rover Evoque prototype (Fig. 1) of the European Union funded project iCOMPOSE.

Fig. 1. The iCOMPOSE vehicle demonstrator: front view with the Corrsys Datron sensor installed across from the front bumper (Lommel Proving Ground, Belgium).

The vehicle demonstrator features four identical on-board drivetrains, each of them consisting of a switched reluctance electric motor, a double-stage single-speed transmission system, constant velocity joints and a half-shaft. The main vehicle parameters are shown in Table 1.

The sensing equipment includes:

- a Corrsys Datron S-350 sensor, installed on the front end of the car (see Fig. 1), providing the vehicle sideslip angle β_{DAT} and the vehicle speed V;
- an Inertial Measurement Unit (IMU), providing longitudinal acceleration a_x, lateral acceleration a_y, and vehicle yaw rate r;
- wheel speed sensors, providing the angular speed of each wheel, i.e. ω_{ij} with $i = F, R$ (front, rear) and $j = L, R$ (left, right);
- a steering wheel angle sensor, providing the steering angle applied by the driver δ;
- a battery current sensor.

Table 1. Main vehicle parameters.

Symbol	Name and unit	Value
m	Mass (kg)	2290
a_1	Front semi-wheelbase (m)	1.365
l	Wheelbase (m)	2.665
τ	Transmission system ratio (-)	10.56
R_w	Wheel radius (m)	0.364
w	Track width (m)	1.616

The tests consisted of ramp steers executed at 30 km/h, 60 km/h and 80 km/h. The different vehicle layouts were: i) FWD; ii) RWD; and iii) AWD with 50:50 front-to-rear wheel torque distribution. In all cases the wheel torques were evenly distributed among the left- and righthand side wheels. Front-to rear and left-to-right distributions were set through the dSPACE AutoBox system installed on the vehicle. The desired vehicle speed was maintained throughout the maneuver by means of a PI (Proportional Integral) speed tracking controller, comparing the desired speed against the average of the four wheel speeds.

The tests were executed according to the following steps:

i) the vehicle was accelerated from standstill to the desired speed in a straight line, using the PI speed tracking controller;

ii) when the desired speed was reached, a ramp steer with constant steering wheel angle rate ($\approx$ 2 deg/s) was applied by the driver;

iii) the test was stopped when the vehicle yaw rate saturated, i.e. the yaw acceleration dropped to zero;

Steps i)-iii) were repeated for all the three specified vehicle speeds and the three wheel torque distributions.

3 RESULTS AND DISCUSSION

3.1 *Data post processing*

The relevant vehicle dynamics quantities were worked out starting from the measured quantities and the geometry of the vehicle, using a simple single-track model (Genta 1997) and the adapted ISO sign convention (Pacejka 2006). Each measured signal was adequately filtered to wipe off the measurement noise (Fig. 2).

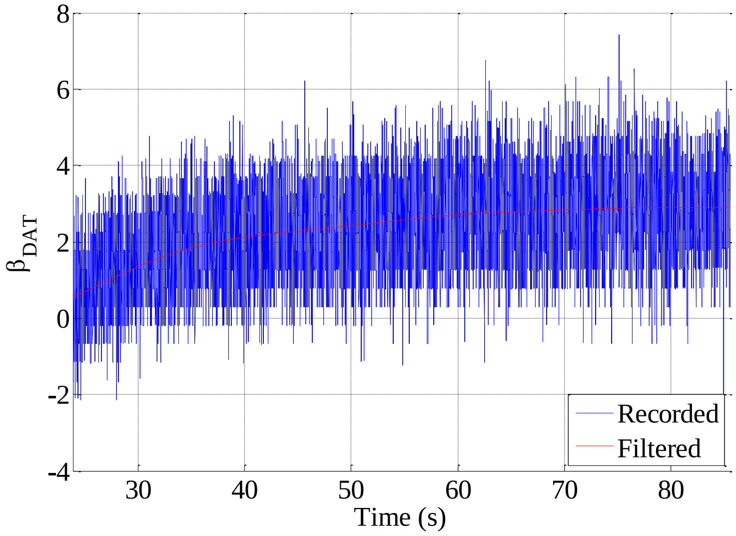

Fig. 2. Comparison between a sample signal as recorded (raw) against the same signal post filtering.

The value of sideslip angle at the center of mass of the vehicle (β_{CG}, this location is the most commonly used in the literature) was obtained by combining the sideslip angle measured by the Datron sensor (β_{DAT}) with the vehicle yaw rate (r), according to the following relationship (Genta 1997, Guiggiani 2014):

$$\tan \beta_{CG} = \tan \beta_{DAT} - \frac{r}{u}(d + a_1) \tag{1}$$

d being the distance between the front axle of the vehicle and the Datron sensor, measured along the longitudinal axis of the vehicle.

As the steering ratio of the car is not constant, a full map was used, providing the left and right wheel steering angles as a function of the steering angle δ applied by the driver. The value of wheel steering angle used for the single-track model was the average of the left and right steering angles.

3.2 *Handling diagram and vehicle dynamics maps analysis*

Figure 3 depicts, for all the vehicle speeds considered, the dynamic steering wheel angle (i.e., the difference among the slip angles at the front and rear axle when using a single-track model) as a function of lateral acceleration. The curves are grouped three by three (for each speed), and they are fairly similar at low lateral acceleration. This holds also at high lateral accelerations at 60 km/h and 80 km/h.

A significant difference in the handling behavior of the vehicle is observed at low speed and high lateral acceleration, with the RWD vehicle clearly resulting more understeering than the FWD vehicle at 30 km/h.

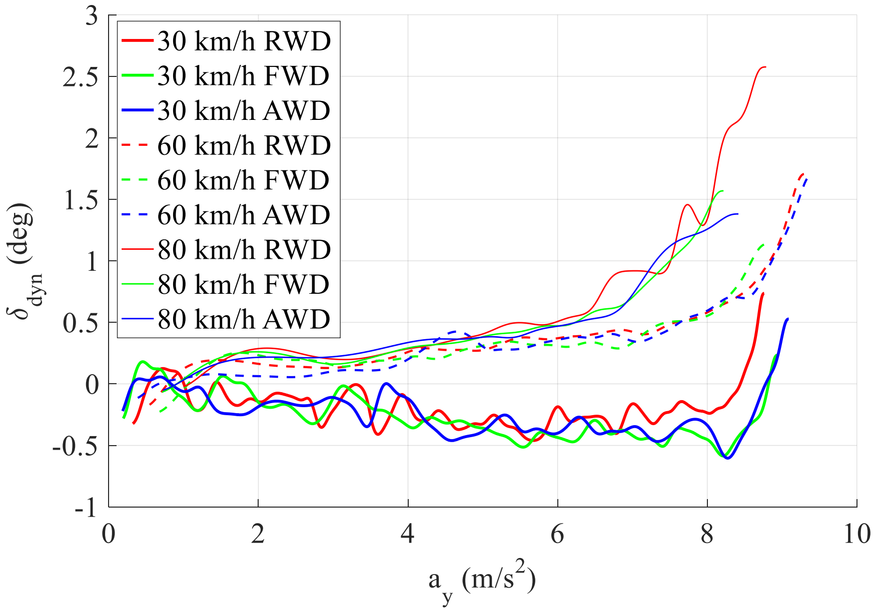

Fig. 3. Dynamic steering wheel angle as a function of the vehicle lateral acceleration.

This apparently surprising result is related to the front longitudinal forces causing a yaw moment because of the steering angle δ_1. To quantify this effect, the longitudinal force X_1 is estimated from the torque demand at front wheels T_{11} and T_{12}, the efficiency of the drivetrain η and the tire radius R_w, which is assumed constant. Consequently, considering the single-track model, the yawing contribution of the longitudinal force N_f is expressed by Eq. 2.

$$N_f = X_1\, a_1 \sin\delta_1 \approx \eta(T_{11} + T_{12})/R\, a_1 \sin\delta_1 \quad (2)$$

It is worth noting that N_f rises as either X_1 or δ_1 rise and consequently N_f is greater at high steering angles and low speeds. Indeed, the lateral force of the front tires is not aligned with the vehicle lateral axis, hence a rearward component is present. The more the lateral acceleration and steering angle values, the more the longitudinal traction force increases, so as to keep the vehicle speed constant by counterbalancing this rearward force.

This trend is also experimentally confirmed in Fig. 4 which shows N_f against a_y for the FWD vehicle and different speed values. At 30 km/h, the yawing contribution N_f rises sharply as the lateral acceleration rises, while at 60 km/h and 80 km/h the curves are almost overlapped, presumably because at higher speed the contribution of the aerodynamic force, requiring a higher value of X_1 to keep the speed constant, is counterbalanced by the lower steering angle δ_1.

Besides the definition of the over/understeer, an alternative approach to the quasi-steady state vehicle dynamics was introduced in (Guiggiani 2014) through the definition of the MAP (Map of the Achievable Performance), where two state variables are plotted one against each other. In Fig. 5 β_{CG} is plotted against the trajectory curvature ρ, for the different vehicle layouts and speed values.

As predictable, the curves are grouped together three by three, depending on the speed value. In particular, at 30 km/h β_{CG} is positive in the whole trajectory curvature range and is almost always rising with the trajectory curvature. On the contrary, at 60 km/h and 80 km/h, β_{CG} is negative and decreases as the trajectory curvature rises.

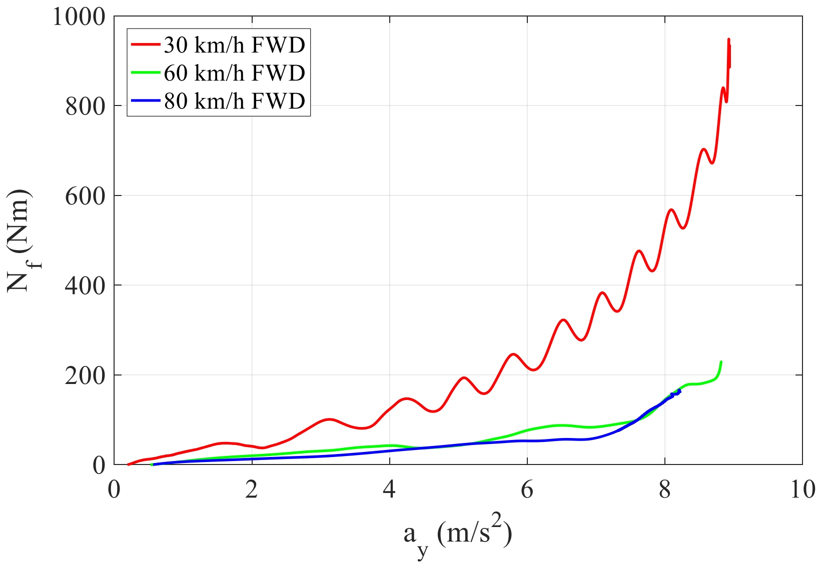

Fig. 4. Yaw moment contribution due to front longitudinal forces for different velocities.

Furthermore, considering each speed value separately, the FWD and AWD curves are almost overlapped along all the trajectory curvature range, while the RWD curve is usually slightly lower, especially at high lateral acceleration.

Fig. 5. Map of the sideslip angle as a function of the curvature radius, for all the tested configurations (improve quality and make uniform style).

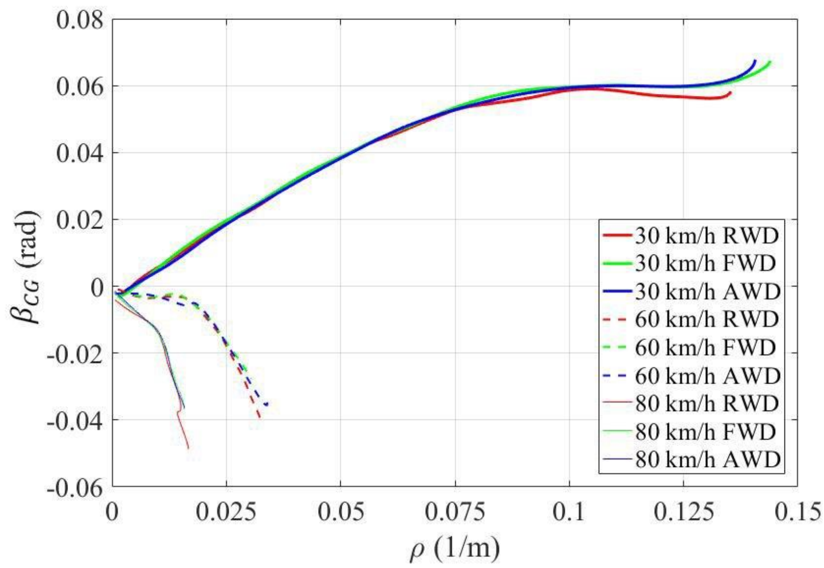

This difference could be justified considering the definition β_{CG} given in Eq. 3, based on the single-track model

$$\beta_{CG} = a_2\rho - \alpha_2 \tag{3}$$

hence, for a given value of the trajectory curvature ρ, the side slip angle β depends only on the slip angle of the rear wheels α_2. It is fair to assume that, comparing the maneuvers at the same speed and same trajectory curvature, the total lateral force of the rear axle Y_2 is the same for the different vehicle layouts. Since the combined effect of traction and lateral force reduces the achievable lateral force given the tire slip angle, the reference lateral force Y_2 is obtained at higher rear slip angle α_2 in the case of RWD.

4 CONCLUSION

The experimental study presented in this paper highlighted how different front-to-rear torque distributions can affect the cornering behavior of a vehicle. The main cause appears to be found in the yaw moment generated by the lateral component of traction forces. Such effect applies regardless of the vehicle being equipped, or not, with a DYC feature.

It was found that the more the steering angle, the more such effect is important. For the case study vehicle demonstrator, at the speed of 30 km/h, the RWD configuration resulted significantly more understeering than the FWD one.

Future studies should analyze the effect of all the individual yaw moment contributions, i.e. due to i) the lateral contribution of traction forces (the only one analyzed in this study); ii) tire lateral forces; iii) self-aligning moment.

5 ACKNOWLEDGEMENT

The research leading to these results has received funding from the European Union Seventh Framework Programme FP7/2007-2013 under Grant Agreement No. 608897 (iCOMPOSE project).

REFERENCES

Bucchi F., Frendo F. 2016. A new formulation of the understeer coefficient to relate yaw torque and vehicle handling. *Vehicle System Dynamics*, 54(6): 831-847.

De Novellis, Sorniotti A., Gruber P. 2014. Design and comparison of the handling performance of different electric vehicle layouts. *Proceedings of the Institution of Mechanical Engineers, Part D: Journal of Automobile Engineering*, 228(2): 218-232.

De Novellis L., Sorniotti A., Gruber P., Orus J., Fortun J. M. R., Theunissen J., De Smet J 2015. Direct yaw moment control actuated through electric drivetrains and friction brakes: Theoretical design and experimental assessment. *Mechatronics*, 26: 1-15.

Frendo F., Greco G., Guiggiani M. 2006. Critical review of handling diagram and understeer gradient for vehicles with locked differential. *Vehicle System Dynamics*, 44(6): 431–447.

Frendo F., Greco G., Guiggiani M., Sponziello A. 2007. The handling surface: a new perspective in vehicle dynamics. *Vehicle System Dynamics*, 45(11): 1001-1016.

Genta G. 1997. *Motor vehicle dynamics: modeling and simulation*. Singapore: World Scientific.

Guiggiani M. 2014. *The science of vehicle dynamics: handling, braking, and ride of road and race cars*. London: Springer Science & Business Media.

Lenzo B., Sorniotti A., De Filippis G., Gruber P., Sannen K. 2016. Understeer characteristics for energy-efficient fully electric vehicles with multiple motors. *EVS29 International Battery, Hybrid and Fuel Cell Electric Vehicle Symposium Proceedings*.

Lenzo B., Sorniotti A., Gruber P., Sannen K. 2017. On the experimental analysis of single input single output control of yaw rate and sideslip angle. *International Journal of Automotive Technology*, in press.

Osborn R. P., Shim T. 2006. Independent control of all-wheel-drive torque distribution. *Vehicle System Dynamics*, 44(7): 529–546.

Pacejka, H. B. 1973. Simplified analysis of steady-state turning behaviour of motor vehicles. Part 1. Handling diagrams of simple systems. *Vehicle System Dynamics*, 2(3): 161–172.

Pacejka H. B. 2006. *Tyre and vehicle dynamics*. Oxford: Butterworth-Heinemann.

Shibahata Y., Shimada K., Tomari T. 1993. Improvement of vehicle maneuverability by direct yaw moment control. *Vehicle System Dynamics*, 22(5–6): 465–481.

Van Zanten, A. T. 2000. Bosch ESP systems: 5 years of experience. *SAE Technical Paper*, 2000-01-1633.